5

Diagnosis of diesel engines

In order to develop advanced fault-detection and diagnosis systems for diesel engines a modular structure is used, which is based on the available input and output signals from the ECU and comprises the actuators and engine components and their sensors, compare Tables 3.3.1 to 3.3.4 and Fig. 3.1.7. Then, so called *detection modules* are defined which allow the fault detection of the interacting components by using their signal readings. This leads to the detection modules for the intake system, injection, combustion, and exhaust system, as shown in Fig. 5.0.1. The detection modules generate certain symptoms as deviations of features from the normal (fault-free) behavior. These symptoms are then the basis of the fault diagnosis for the overall engine, using fault-symptom relationships for the components of the engine and their interrelations indicating the type and location of the faults.

An improvement of engine diagnosis systems over the implemented OBD functions is obtained by using the inherent properties of measured signals and relations between the signals. Therefore, model-based methods are described in the following sections which use both, *signal models* and *process models*. These models must be able to express the influence between faultless and faulty behavior. Because only relatively few measured signals are available in mass-production engines a grouping into the mentioned detection modules will be made.

Several signals are periodic because of the repetitive cylinder charging and combustion operations. Hence, methods of harmonic signal analysis, like Fourier or Wavelet analysis, can be applied. The process models, relating input and output signals, use as a basis physical models, which have to be simplified, because of real-time computational demands. However, as physically based models of the engine include nonlinear fluidic and thermodynamic processes many parameters have to be estimated experimentally, because they are not known in advance and vary strongly. Then it may be more straightforward to use process models based on identification and parameter-estimation methods. If the structure of these models is based on simplified physical models, this results in semi-physical models, Töpfer et al (2002). Because of the strongly nonlinear behavior of combustion engines, also neural-network approaches may be used. Here, a practical feasible type is the use of local linear models, based on parameter-estimation methods and weighting with radial basis func-

R. Isermann, *Combustion Engine Diagnosis*, ATZ/MTZ-Fachbuch, DOI 10.1007/978-3-662-49467-7_5

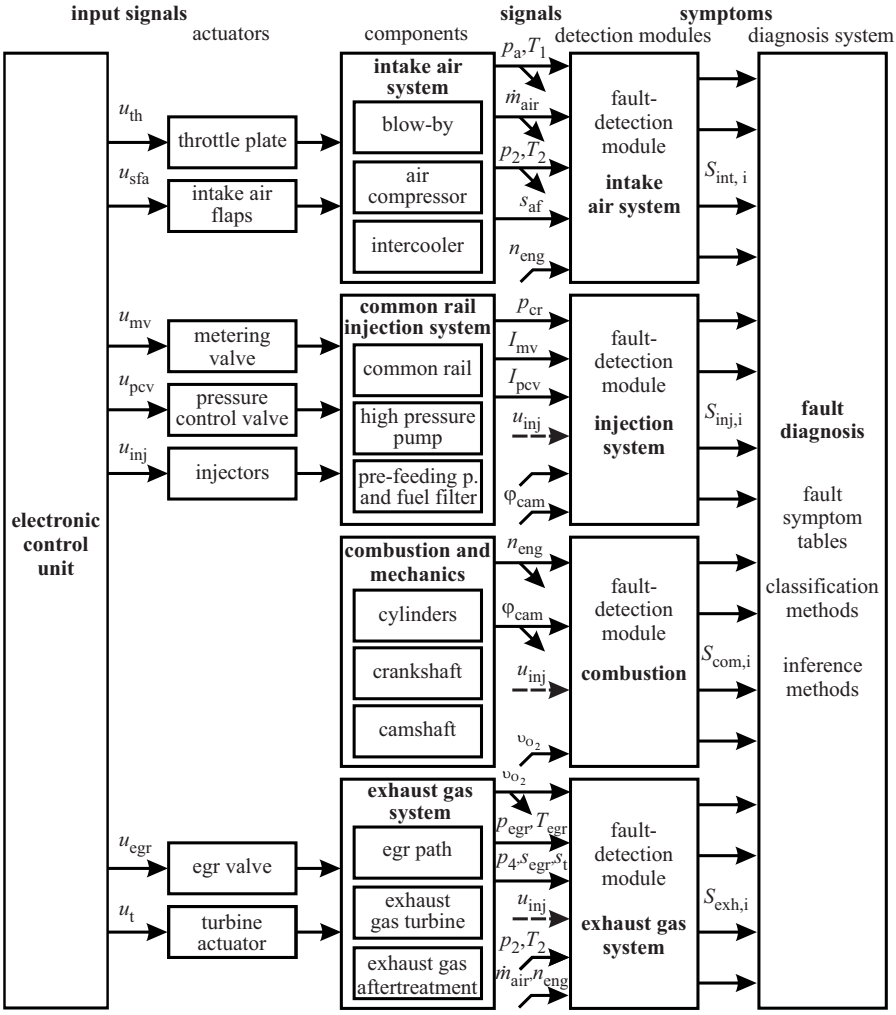

Fig. 5.0.1. Modular structure of a diesel-engine fault-diagnosis system with four detection modules.

tions (e.g. LOLIMOT method). The procedure described in the next sections was mainly developed by Schwarte et al (2004), Kimmich (2004), Kimmich et al (2005), Clever (2011), Eck et al (2011), and Sidorow (2014).

The available sensor signals depend on the type of the diesel engine. A first difference comes from the kind of fuel injection. *Cam-driven distributor injection pumps* with axial or radial pistons for all cylinders or *unit injector pumps* for each cylinder possess solenoid valves for determining pilot injection, main injection and post injection. The electronic control is either integrated in the pump device or part of the engine ECU and uses (internally) in addition to the begin of injection and the fuel

5.3 Common-rail injection system

High pressure injection systems play a central role in any direct injection internal combustion engine. Many faults, malfunctions and failures of the engines origin in the highly stressed injection pump, common-rail pressure control and injectors. Therefore, it is of considerable interest to detect and diagnose early incipient faults before they lead to intermittent and permanent drastic faults and even failures of the injection followed by failures of the combustion process.

In the frame of the OBD diagnosis the injection system is already supervised with regard to some emission-related faults. Hence, larger faults of the sensors, the rail pressure control deviations and wire connections are already checked and examined for plausibility. However, a detailed fault detection and diagnosis is usually not provided.

In the following a model-based fault-detection module for an electronically controlled common-rail injection system for diesel engines is described. It is the result of an in-depth case study, Clever and Isermann (2008), Clever (2010), Clever and Isermann (2010), Clever (2011). The investigated injection system is the type CP1H from Bosch. A corresponding scheme is depicted in Fig. 5.3.1. Measurements are made on a test bench with a four-cylinder diesel engine, Opel/GM, 1.9l, 110 kW, 315 Nm, as depicted in Fig. 5.4.1a).

The dynamic models of the components of a high pressure common-rail system were already established in Isermann (2014), Sect. 5.5.3, resulting in the signal flow chart, Fig. 5.3.2, for the common-rail pressure.

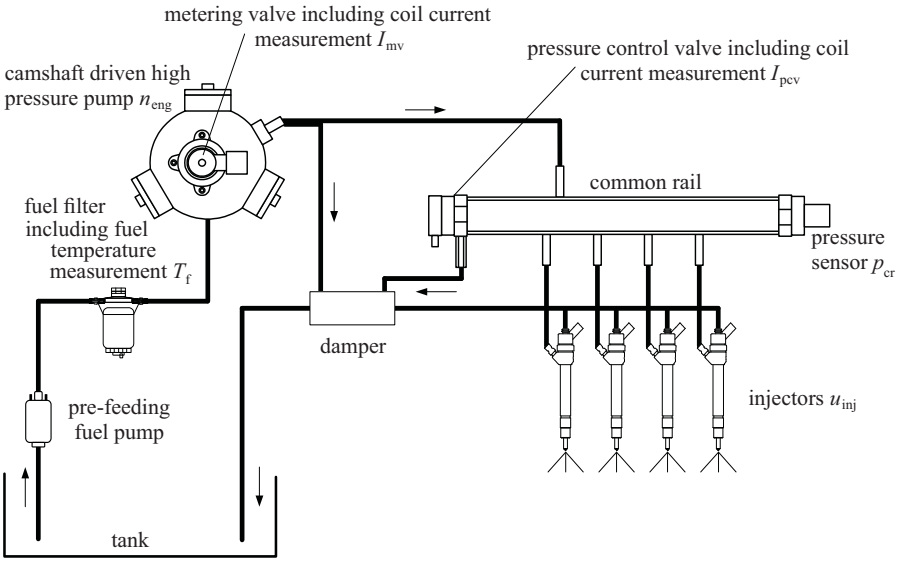

Fig. 5.3.1. Scheme of a common-rail injection system.

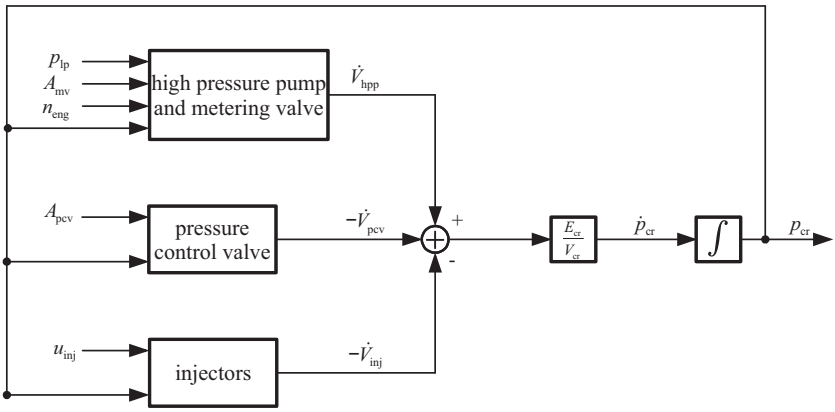

Fig. 5.3.2. Signal flow chart for the common-rail pressure, Isermann (2014).

5.3.1 Analysis of the rail pressure signal

The common-rail pressure consists of a mean value according to the reference variable of the pressure control loop and periodic oscillations through the discontinuous delivery of the radial piston pump and periodic opening and closing of the injectors. The mean value as well as the oscillation are subject to changes if faults in the injection system arise. Before corresponding fault-detection features are stated, first the signal characteristics of the oscillations are analyzed.

Because these oscillations are composed of periodic signals with different frequencies, they are modeled by a Fourier series

$$y(t) = \frac{a_0}{2} + \sum_{\nu=1}^{\infty} a_\nu \cos(\nu\omega_0 t) + \sum_{\nu=1}^{\infty} b_\nu \sin(\nu\omega_0 t) \tag{5.3.1}$$

with

a_ν, b_ν	Fourier coefficients
$\omega_0 = 2\pi f_0$	characteristic angular frequency
f_0	fundamental frequency.

The Fourier coefficients are defined as

$$a_\nu(\nu\omega_0) = \frac{2}{T_\mathrm{p}} \int_0^{T_\mathrm{p}} y(t) \cos(\nu\omega_0 t) dt, \tag{5.3.2}$$

$$b_\nu(\nu\omega_0) = \frac{2}{T_\mathrm{p}} \int_0^{T_\mathrm{p}} y(t) \sin(\nu\omega_0 t) dt. \tag{5.3.3}$$

The time period T_p needs to be a multiple of the fundamental period

$$T_\mathrm{p} = r \frac{1}{f_0}, \quad r = 1, 2, \ldots \tag{5.3.4}$$

Given the Fourier coefficients, the amplitude of the oscillation for a characteristic angular frequency can be calculated by

$$A_y(\nu\omega_0) = \sqrt{a_\nu^2 + b_\nu^2}. \tag{5.3.5}$$

In order to get the coefficients from sampled data, (5.3.1) has to be discretized:

$$a_\nu(\nu\omega_0) \approx \frac{2}{L_\mathrm{p}} \sum_{k=0}^{L_\mathrm{p}-1} y(kT_0) \cos(\nu\omega_0 k T_0), \tag{5.3.6}$$

$$b_\nu(\nu\omega_0) \approx \frac{2}{L_\mathrm{p}} \sum_{k=0}^{L_\mathrm{p}-1} y(kT_0) \sin(\nu\omega_0 k T_0), \tag{5.3.7}$$

$$L_\mathrm{p} = \frac{T_\mathrm{p}}{T_0}, \tag{5.3.8}$$

where T_0 is the sampling time and N the signal length.

Figure 5.3.3 shows the amplitude spectra of a common-rail pressure sensor signal while the engine was in a stationary operation point in overrun (no fuel injections) and the common-rail pressure was in open loop. The values of the main variables for the operation condition are also shown. The shown measurement is mainly characterized by an oscillation with the angle period

$$\text{main pump cycle:} \qquad \tau_\mathrm{pist} = 180^\circ\mathrm{CS}. \tag{5.3.9}$$

This oscillation is forced by the high pressure pump. Because the radial piston pump consists of three pistons, and is driven by the camshaft belt at a ratio of 2:3 relating to the crankshaft, each $180^\circ\mathrm{CS}$ one pump element delivers fuel leading to the main pump cycle.

Usually, the three pump elements deliver the same amount of fuel in a stationary operation point. If the delivery quantity of at least one element differs, an additional oscillation appears (see Fig. 5.3.4). Since each of the three pump elements delivers fuel once in $540^\circ\mathrm{CS}$, the cycle angle of this oscillation is

$$\text{second pump cycle:} \qquad \tau_\mathrm{hpp} = 540^\circ\mathrm{CS}. \tag{5.3.10}$$

If fuel is injected, the considered four-cylinder engines opens the injectors each $180^\circ\mathrm{CS}$, yielding the

$$\text{main injection cycle:} \qquad \tau_\mathrm{inj} = 180^\circ\mathrm{CS} \tag{5.3.11}$$

which has the same cycle angle as the main pump cycle, see Fig. 5.3.5.

If the volume flow to at least one injector differs due to different recycle flows or injection quantities, the cycle angle of additional oscillations becomes

$$\text{second injection cycle:} \qquad \tau_\mathrm{bank} = 720^\circ\mathrm{CS}. \tag{5.3.12}$$

This second injection cycle now differs from the second pump cycle.

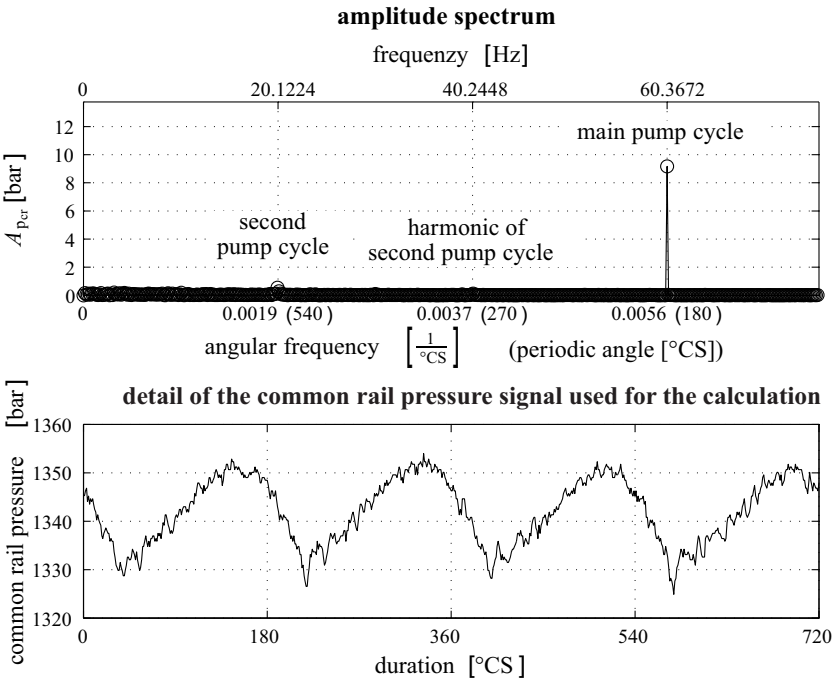

operation point

common rail pressure controlled in open loop

essential variables	n_{eng}	$\dot{V}_{inj}$	I_{pcv}	I_{mv}
values	≈1800 rpm	$0\frac{mm^3}{cyl}$	1.05A	0.87A

Fig. 5.3.3. Measured common-rail pressure signal and its amplitude spectrum in overrun. The basic oscillation is forced by the three pump elements of the camshaft belt driven radial piston pressure pump.

If the delivery quantity of at least one of the three pump elements is different from the others and at the same time the volume flow to at least one of the four injectors differs from the others, all of the above discussed oscillations are present in the signal but have different amplitudes. This leads to several combinations of different fuel delivery quantities on the one hand and different volume flows to the injectors on the other. These combinations repeat after the period

$$\text{superimposed cycle: } \tau_{sup} = \tau_{hpp,bank} = 3 \cdot 4 \cdot 180°\text{CS} = 2160°\text{CS}. \quad (5.3.13)$$

Because the amplitudes of the common-rail pressure oscillations forced by the high pressure pump and the injections are small compared to the mean common-rail pressure, it can be assumed that the volume flows through the pressure control valve and through the leakages are constant for a stationary operating point:

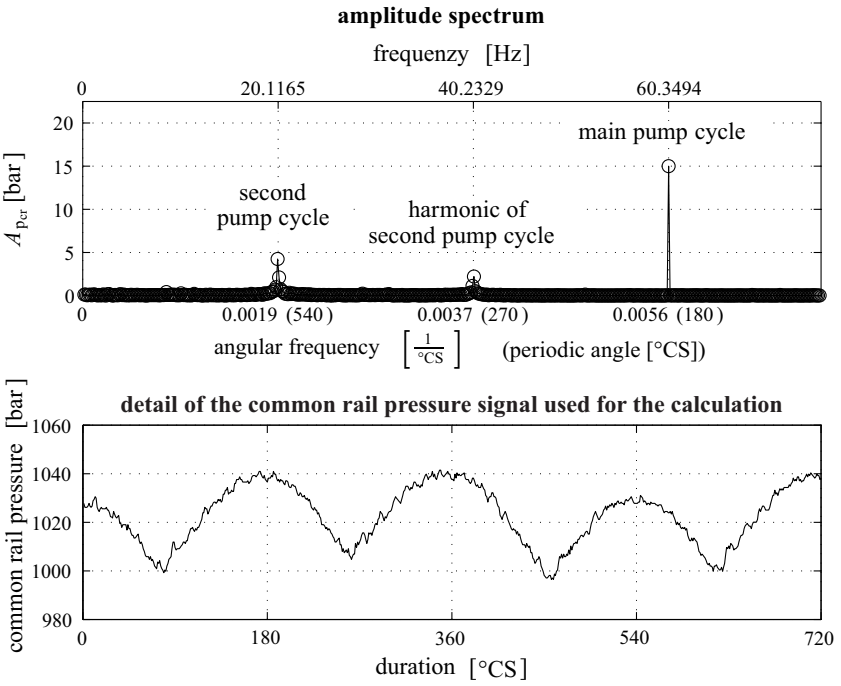

operation point

common rail pressure controlled in open loop

essential variables	n_{eng}	$\dot{V}_{\mathrm{inj}}$	I_{pcv}	I_{mv}
values	≈1800 rpm	$0\frac{\mathrm{mm}^3}{\mathrm{cyl}}$	1.15A	0.72A

Fig. 5.3.4. Measured common-rail pressure signal and its amplitude spectrum in overrun. One pump piston delivers less fuel, leading to a second pump cycle with period $540°\mathrm{CS}$.

$$V_{\mathrm{pcv}} + V_{\mathrm{leak}} \approx \text{constant for a stationary operation point.} \tag{5.3.14}$$

Thus, these volume flows do not cause additional oscillations of the common-rail pressure. Figure 5.3.6 illustrates the discussed oscillations with the cycle angles τ_{inj}, τ_{bank}, τ_{pist}, τ_{hpp} and τ_{sup}.

The amplitude of the main pump oscillation at $180°\mathrm{CS}$ depends on the delivered fuel and angular speed. The delivered fuel to the high pressure pump from the low pressure pump is feedforward controlled by the metering valve. This valve determines the fuel flow rate to the pump in order to save pumping energy and unnecessary heating-up of the fuel, Robert Bosch GmbH (2005). Therefore, the high pressure pump has some non-delivery rotation angles $0 \leq \chi \leq 180°\mathrm{CS}$. As shown in Clever (2011), the amplitudes of the common-rail pressure change in dependence on the engine speed and metering valve position respectively valve current

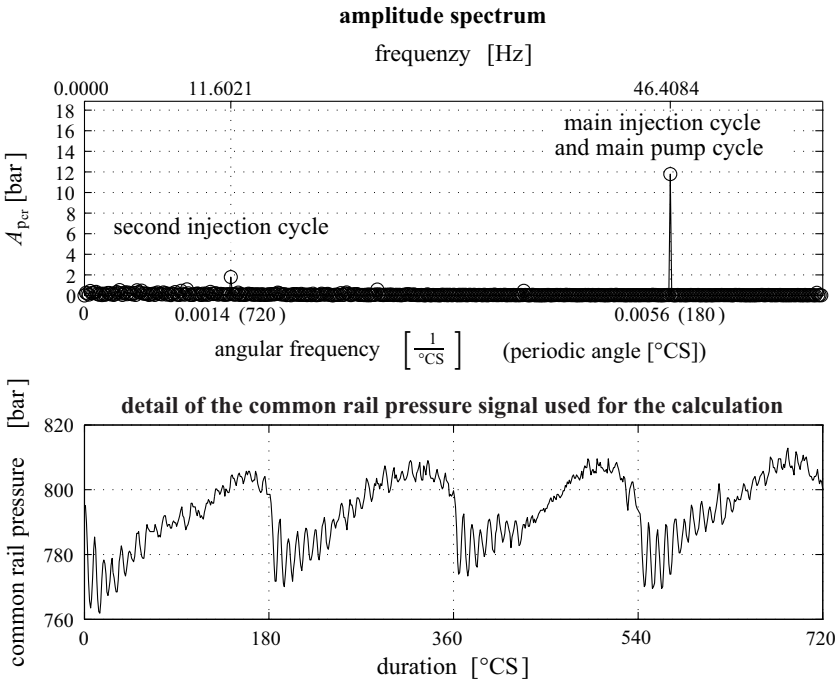

operation point

common rail pressure controlled in open loop

essential variables	n_{eng}	$\dot{V}_{\text{inj}}$	I_{pcv}	I_{mv}
values	≈1300 rpm	≈20.02 $\frac{\text{mm}^3}{\text{cyl}}$	1.05A	0.80A

Fig. 5.3.5. Measured common-rail-pressure signal and its amplitude spectrum for active injectors. One injector injects more fuel than the others, leading to a second injection cycle with period $540°\text{CS}$.

$4\,\text{bar} \leq A_{\text{pcr}}(180°\text{CS}) \leq 15\,\text{bar}$ for overrun and can be represented as normal values in a look-up table.

The measured oscillations of the common-rail pressure finally are a superposition of the individual induced oscillations by the high pressure pump and the injectors. The superposition leads to following measurable periods:

$$\begin{aligned} &\text{first sum period} && \tau_{\text{pist,inj}} = 180°\text{CS} \\ &\text{second pump period} && \tau_{\text{hpp}} = 540°\text{CS} \\ &\text{second injector period} && \tau_{\text{bank}} = 720°\text{CS} \\ &\text{second sum period} && \tau_{\text{hpp,bank}} = 2160°\text{CS} \end{aligned} \tag{5.3.15}$$

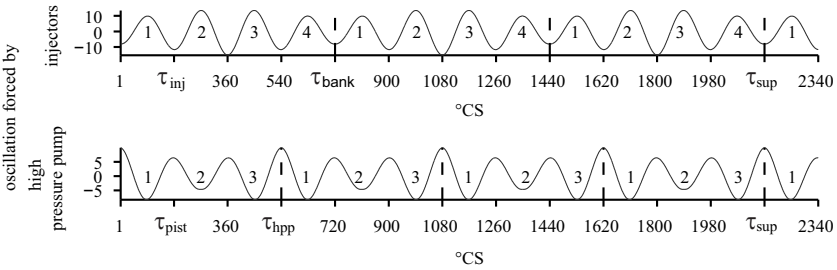

Fig. 5.3.6. Illustration of the oscillations forced by the volume flows through the high pressure pump and the injectors. (Each number indicates the injector which is currently active and the pump element which currently delivers fuel, respectively. In order to illustrate the oscillations caused by differences of the volume flows to the injectors on the one hand and differences of the delivery quantities of the three pump elements on the other, different amplitudes of the forced oscillations are assumed. For the injector flows it is assumed that the volume flows to the injectors 1 and 4 are smaller than the flows to the injectors 2 and 3. For the delivery quantities of the pump elements it is assumed that the delivery quantity of pump element 2 is smaller than the delivery quantities of the other pump elements).

where it holds for the resulting frequencies with $f = n_{\mathrm{eng}}\tau/360$. For $n_{\mathrm{eng}} = 1800\mathrm{rpm} = 30\mathrm{rps}$ one obtains

$$\begin{aligned} &\text{first sum frequency} && f_{\mathrm{pist,inj}} = 60\mathrm{Hz} \\ &\text{second pump frequency} && f_{\mathrm{hpp}} = 20\mathrm{Hz} \\ &\text{second injector frequency} && f_{\mathrm{bank}} = 15\mathrm{Hz} \\ &\text{second sum frequency} && f_{\mathrm{hpp,bank}} = 5\mathrm{Hz} \end{aligned} \tag{5.3.16}$$

5.3.2 Model-based fault diagnosis

A failure mode and effect analysis (FMEA) with faults of the fuel filter, metering valve, pump mechanics, pressure control valve, injector including seals and possible failure effects on the engine is reported in Clever (2011). Based on this analysis, artificially introduced faults have been selected for experiments.

The fault detection is based on output residuals between measured or calculated quantities and their normal values, see Fig. 5.3.7.

a) Mean common-rail pressure

Figure 5.3.2 shows the used signal flow diagram of the pressure build-up in the common-rail. In order to remove the oscillations of the common-rail signal, it is low-pass filtered.

Based on physical modeling leading to the model structure, a common-rail pressure model can be identified from measured data. But not all of the inputs in Fig. 5.3.2 are available as measurements. For this reason the model structure, depicted in

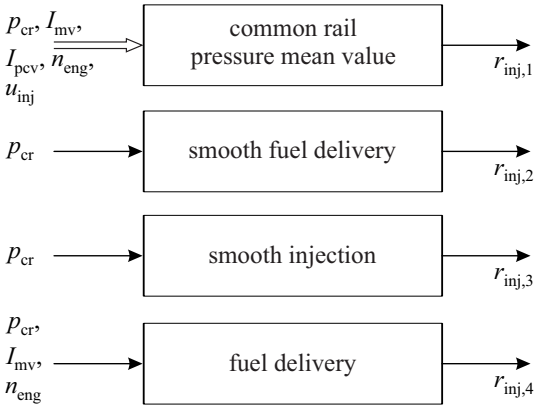

Fig. 5.3.7. Measured input variables and residuals for the model-based fault detection of the common-rail injection system.

Fig. 5.3.8, is used. It is assumed that the pressure before the metering valve is constant. Thus, it is not used as an input for the model anymore. Further it is assumed that the opening cross section of the metering valve and the pressure control valve are approximately proportional to the measured current through the electromagnetic actuators. Thus, the measured currents through the two valves are used as model inputs. The hysteresis of the position of the pressure control valve is taken into account by offset values for the maximum hysteresis width.

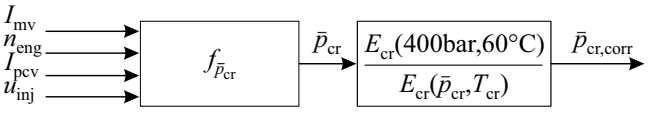

Fig. 5.3.8. Signal flow scheme for the common-rail pressure with used measured input signals.

By means of a model for the bulk modulus, the measured common-rail pressure is related to a bulk modulus at a particular pressure (e.g. 400 bar) and at a certain temperature (e.g. 60°C). Also the fuel temperature is calculated based on a model.

The data-based modeling and identification of the common-rail pressure is conducted using the net model LOLIMOT with the inputs:

I_{mv}	supply current of the metering valve
I_{pcv}	supply current of the pressure control valve
n_{eng}	engine speed
u_{inj}	desired injection quantity

On basis of the estimated model following parity equation for the “mean common-rail pressure” can be formulated:

Table 5.3.2. Fault-symptom table for the common-rail system. $0, +, -$: symptom is zero, positive, ✓, ×: yes, no.

		$S_{\mathrm{inj},1}$	$S_{\mathrm{inj},2}$	$S_{\mathrm{inj},3}$	$S_{\mathrm{inj},4}$	$S_{\mathrm{inj},5}$	$S_{\mathrm{inj},6}$	isolable
$F_{\mathrm{inj},1}$	low delivery quantity of one pump piston	0	+	0	+	−	+	✓
$F_{\mathrm{inj},2}$	reduced injection quantity of one injector	0	0	+	0	0	0	✓
$F_{\mathrm{inj},3}$	pressure loss in front of high pressure pump (e.g. a plugged fuel filter)	−	0	0	+	−	+	✓
$F_{\mathrm{inj},4}$	pressure in front of high pressure pump too high (e.g. a faulty metering valve)	+	0	0	+	+	−	✓
$F_{\mathrm{inj},5}$	opening of the pressure control valve is too large	−	0	0	0	0	0	✓
$F_{\mathrm{inj},6}$	opening of the pressure control valve is too small	+	0	0	0	0	0	✓
$F_{\mathrm{inj},7}$	pressure sensor signal is too high	+	0	0	+	−	−	✓
$F_{\mathrm{inj},8}$	pressure sensor signal is too low	−	0	0	+	+	+	✓

are not necessary for the diagnosis. However, since the symptom $S_{\mathrm{inj},4}$ is calculated in a wider operation range, it may be advantageous to use it in the diagnosis procedure in order to be able to diagnose the faults $F_{\mathrm{inj},5}$ and $F_{\mathrm{inj},6}$ earlier.

Table 5.3.2 shows that all faults can be distinguished from each other if the fault detection results are combined in a single fault-detection system.

The fault-detection method for the common-rail system was described for a four-cylinder engine with a three-piston high pressure pump. However, the method can also be adapted to engines with three and five to eight cylinders and high pressure pumps with one or two pistons, Clever (2011).

As the highest frequency respectively the shortest period is $180°\mathrm{CS}$, see (5.3.15), the sampling period should be $\leq 90°\mathrm{CS}$ according to Shannon's sampling theorem. Experiments with a sampling period of $60°\mathrm{CS}$ have shown the same results as in Fig. 5.3.10, Clever (2011). The described fault-diagnosis method was filed to patent, Clever and Isermann (2010).

5.4 Turbochargers with wastegate and variable geometry

As all modern diesel engines and increasingly also gasoline engines are equipped with charging units which are mechanically driven superchargers or exhaust-gas turbochargers, the monitoring and fault diagnosis of these highly stressed components is mandatory. Usually, the charging pressure $p_{2\mathrm{i}}$ and charging air temperature $T_{2\mathrm{i}}$ is measured. Together with the air mass flow rate $\dot{m}_{\mathrm{air}}$ this allows to determine the

power of the compressor with efficiency maps. These maps can be used for fault detection. In the case of turbochargers, the supervision of the turbine power additionally requires the measurements of the exhaust pressure p_3 and exhaust temperature T_3 upstream the turbine, in the exhaust manifold, and several efficiency maps. For modeling turbochargers the steady-state maps delivered from manufacturers can be used. However, they are frequently not precise in the required engine operation range and do not consider the pulsating exhaust gas flow. Therefore more comprehensive and dynamic models of turbochargers will be considered.

As a basis for model-based fault detection the nonlinear dynamic models of variable-geometry turbine (VGT) chargers and wastegate (WG) chargers will be considered in the next section. The models are derived for the diesel engine shown in Fig. 5.4.1a) with the variables shown in Fig. 5.4.1b).

5.4.1 Models of VGT turbochargers

Dynamic models of turbochargers can be derived based on thermodynamic changes of state or based on fluid dynamic approaches by using Euler's equation for turbomachinery. Both modeling ways are described in Isermann (2014), Zahn (2012) and Sidorow (2014). For fault detection thermodynamic models for the turbine and compressor power will now be preferred, because they need fewer parameters to be identified, Sidorow (2014). It is assumed that the engine is in normal warm state.

The dynamic behavior at one operating point $[u_{\mathrm{inj}}, n_{\mathrm{eng}}]$ results from the balance equation for the angular momentum

$$J_{\mathrm{tc}} \frac{d\omega_{\mathrm{tc}}(t)}{dt} = M_{\mathrm{t}}(t) - M_{\mathrm{c}}(t) - M_{\mathrm{f}}(t) \tag{5.4.1}$$

with torques M_{t} for the turbine, M_{c} for the compressor and M_{f} for the friction, see Fig. 5.4.2. Turning the equation to powers with $P = M\omega$ leads to

$$J_{\mathrm{tc}}\, \omega_{\mathrm{tc}}(t)\, \frac{d\omega_{\mathrm{tc}}(t)}{dt} = P_{\mathrm{t}}(t) - P_{\mathrm{c}}(t) - P_{\mathrm{f}}(t). \tag{5.4.2}$$

The friction torque is assumed to be dominated by viscous friction $M_{\mathrm{f}} = c_{\mathrm{f}}\, \omega_{\mathrm{tc}}$ and therefore

$$P_{\mathrm{f}}(t) = c_{\mathrm{f}}(T_{\mathrm{oil}})\, \omega_{\mathrm{tc}}^2. \tag{5.4.3}$$

The *turbine power* follows according to

$$P_{\mathrm{t}} = \dot{m}_{\mathrm{t}}\, c_{\mathrm{pt}}\, T_3^*\, \eta_{\mathrm{t,is}} \left(1 - \left(\frac{p_4}{p_3} \right)^{\frac{\kappa-1}{\kappa}} \right) \tag{5.4.4}$$

with the mass flow determined by a throttle equation

$$\dot{m}_{\mathrm{t}} = A_{\mathrm{t,eff}}\, p_3 \sqrt{\frac{2}{R T_3^*}}\, \psi(\frac{p_4}{p_3}) \tag{5.4.5}$$

$$\psi(\frac{p_4}{p_3}) = \left(\frac{p_4}{p_3} \right)^{\frac{1}{\kappa}} \sqrt{\frac{c_{\mathrm{pt}}}{R} \left[1 - \left(\frac{p_4}{p_3} \right)^{\frac{\kappa-1}{\kappa}} \right]}. \tag{5.4.6}$$

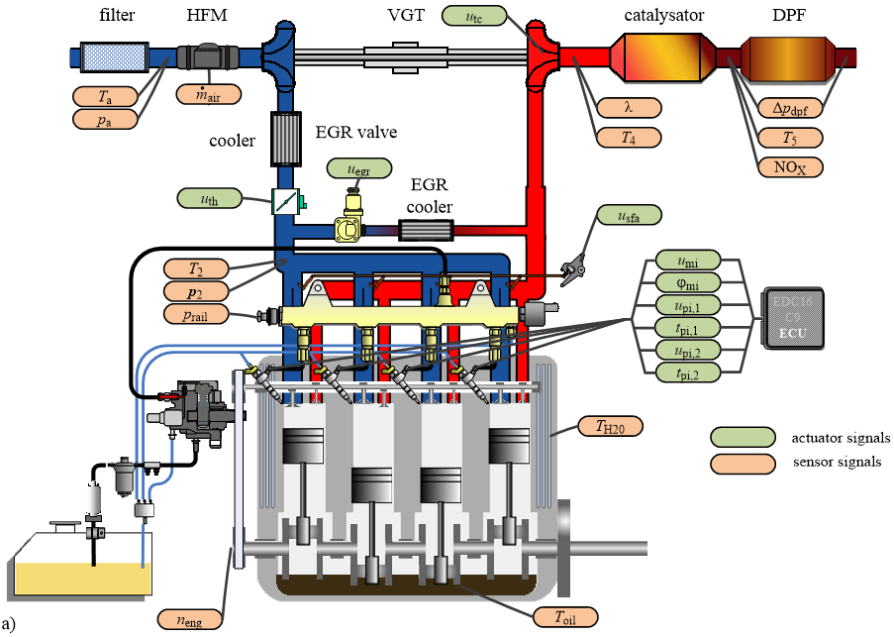

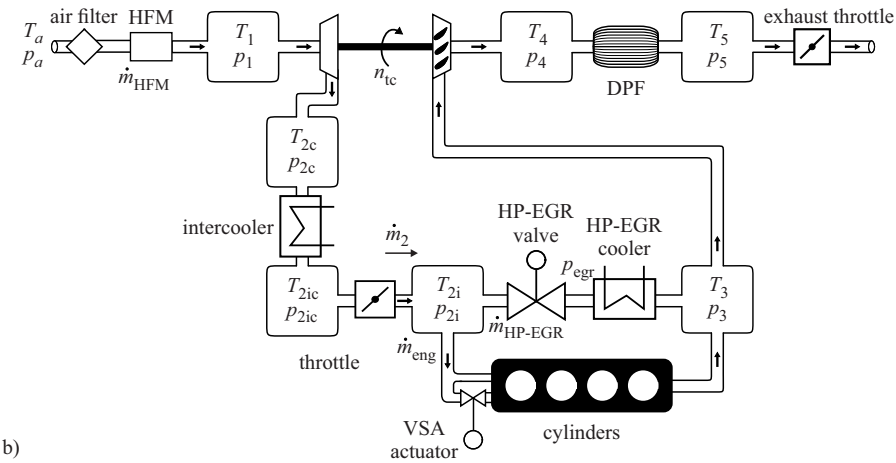

Fig. 5.4.1. a Scheme of the investigated diesel engine with common-rail direct injection and VGT turbocharger, Opel/GM, 1.9*l*, 110 kW, 315 Nm. Actuator and sensor signals as used on the IAT test bench. **b** Used variables for the diagnosis of turbochargers.

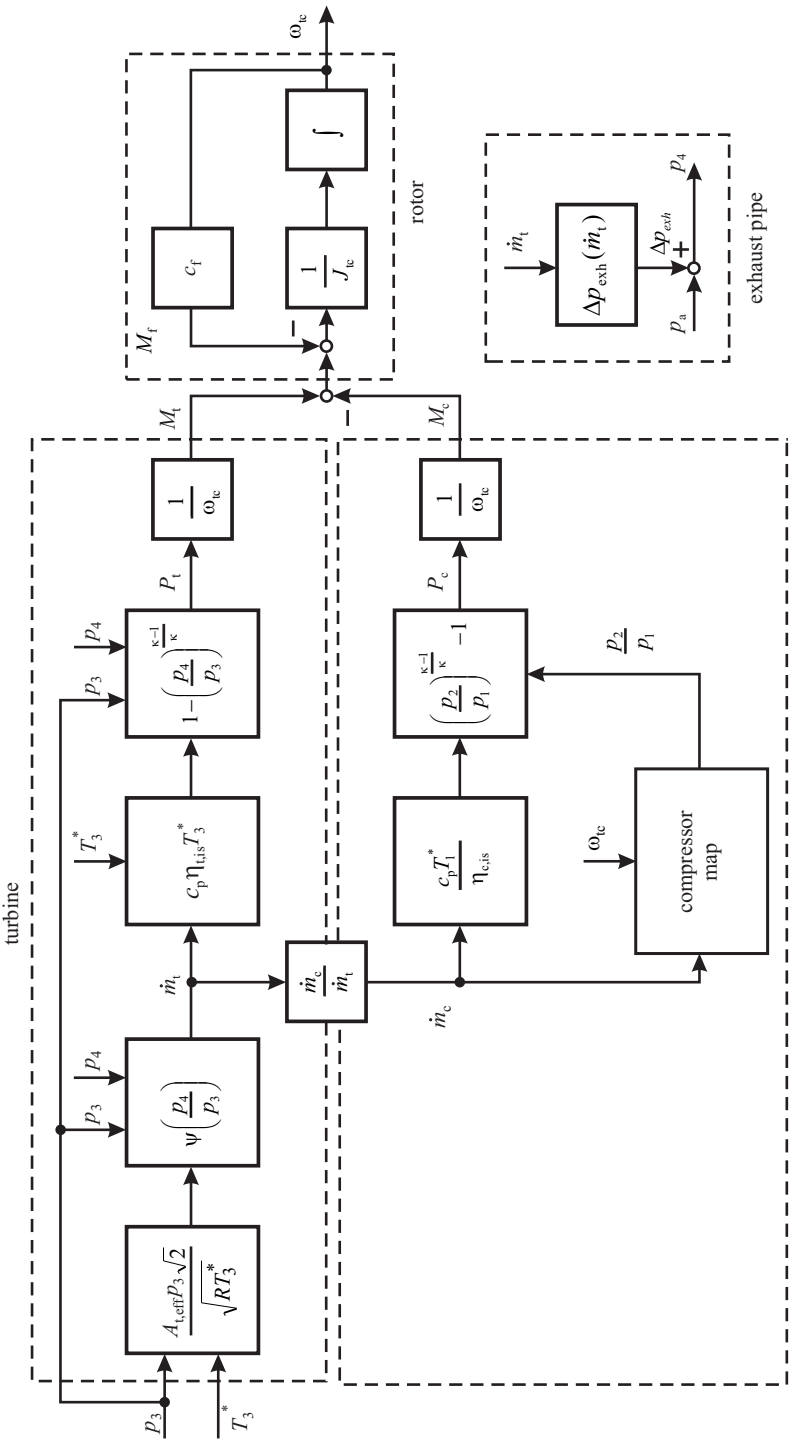

Fig. 5.4.2. Signal-flow chart for the thermodynamic model of a turbocharger (without internal heat transfer).

The effective cross section area $A_{\mathrm{t,eff}}(s_\mathrm{t}, p_4)$ is a function of the actuator position s_t and the pressure p_4 after the turbine. T_3^* is the gas temperature before the turbine reduced by the heat transfer loss to the compressor and the environment.

The isentropic efficiency of the turbine is defined as

$$\eta_{\mathrm{t,is}} = \frac{\frac{T_4}{T_3^*} - 1}{\left(\frac{p_4}{p_3}\right)^{\frac{\kappa-1}{\kappa}} - 1}. \tag{5.4.7}$$

It is difficult to determine this efficiency for low turbocharger mass flows and speeds, because the heat transfer to the compressor becomes effective in these cases. Therefore it is determined experimentally by a map $\eta_{\mathrm{t,is}}(s_\mathrm{t}, u_\mathrm{ref})$, see Fig. 5.4.3, where u_ref is the turbine blade speed ratio, Guzzella and Onder (2010),

$$u_\mathrm{ref} = \frac{u}{c_{\mathrm{u,max}}} = \frac{d_{\mathrm{t}3}\pi}{\sqrt{2c_\mathrm{p}T_3\left(1 - \left(\frac{p_4}{p_3}\right)^{\frac{\kappa-1}{\kappa}}\right)}}\omega_\mathrm{tc},$$

which is proportional to the turbocharger angular speed ω_tc, see also Isermann (2014).

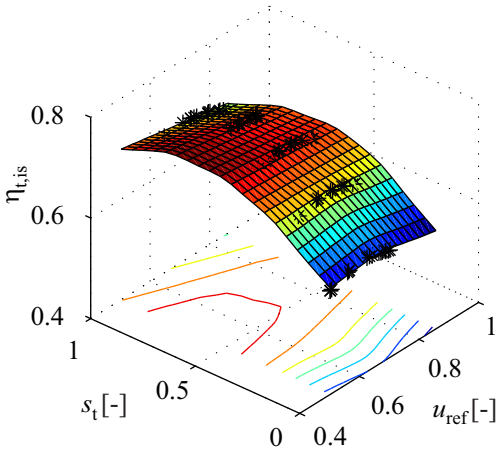

Fig. 5.4.3. Turbine isentropic efficiency map, approximated with a LOLIMOT net model, Sidorow et al (2011).

Hence, following variables have to be measured to calculate the turbine power $P_\mathrm{t}(u_\mathrm{inj}, n_\mathrm{eng})$

$$\mathbf{z}_\mathrm{t}^T = \left[p_3,\, p_4,\, T_3,\, s_\mathrm{t}\right]. \tag{5.4.8}$$

p_4 can be determined by the measured pressure drop of the particulate filter

$$p_4 = p_1 + \Delta p_\mathrm{pf}(\dot{m}_\mathrm{t}). \tag{5.4.9}$$

For larger mass flows, $T_3^* = T_3$ can be assumed. The *compressor power* is

$$P_\mathrm{c} = \dot{m}_\mathrm{c}\, c_\mathrm{pc}\, \frac{T_1^*}{\eta_\mathrm{c,is}} \left(\left(\frac{p_2}{p_1} \right)^{\frac{\kappa-1}{\kappa}} - 1 \right) \tag{5.4.10}$$

where $\dot{m}_\mathrm{c}$ is taken from a compressor mass flow map $\dot{m}_\mathrm{c}(n_\mathrm{tc}, p_2/p_1)$, see Fig. 5.4.4, or is directly measured with $\dot{m}_\mathrm{c} = \dot{m}_\mathrm{air}$.

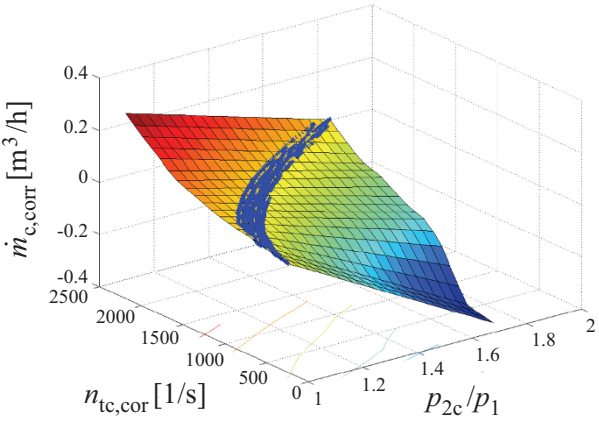

Fig. 5.4.4. Compressor mass flow map.

T_1^* is the inlet temperature, taking into account the heat transfer from the turbine

$$T_1^* = T_1 + \frac{k_{13} A_\mathrm{c}}{c_\mathrm{pc}\, \dot{m}_\mathrm{c}} (T_3 - T_1) \tag{5.4.11}$$

with the heat transfer coefficient k_{13} and the effective surface area A_c.

The isentropic efficiency of the compressor is defined as

$$\eta_\mathrm{c,is} = \frac{\left(\frac{p_2}{p_1} \right)^{\frac{\kappa-1}{\kappa}} - 1}{\frac{T_2}{T_1^*} - 1} \tag{5.4.12}$$

and it is experimentally determined in form of a map $\eta_\mathrm{c,is}(\dot{m}_\mathrm{c}, n_\mathrm{tc})$, see Fig. 5.4.5.

The required measurements needed to calculate the compressor power $P_\mathrm{c}(u_\mathrm{inj}, n_\mathrm{eng})$ are

$$\mathbf{z}_\mathrm{c}^\mathrm{T} = \left[\dot{m}_\mathrm{air},\, T_1,\, p_1,\, p_2 \right]. \tag{5.4.13}$$

To make the turbocharger characteristics independent of the changing environmental conditions, the variables are usually stated as referenced or corrected quantities using fluid mechanical laws. The reference conditions for the compressor inlet are $T_\mathrm{1ref} = 193\mathrm{K}$, $p_\mathrm{1ref} = 0.981\mathrm{bar}$ and for the turbine inlet they are $T_\mathrm{3ref} = 873\mathrm{K}$. This leads to the corrected rotational speed

http://www.springer.com/978-3-662-49466-0

Combustion Engine Diagnosis
Model-based Condition Monitoring of Gasoline and Diesel Engines and their Components
Isermann, R.
2017, XXI, 303 p. 169 illus., 22 illus. in color., Hardcover
ISBN: 978-3-662-49466-0